Distinct RNA polymerase transcripts direct the assembly of phase-separated DBC1 nuclear bodies in different cell lines

Taro Mannen[a,*], Masato Goto[a], Takuya Yoshizawa[a], Akio Yamashita[b], Tetsuro Hirose[c,*], and Toshiya Hayano[a]

[a]College of Life Sciences, Ritsumeikan University, Kusatsu 525-8577, Japan; [b]Graduate School of Medicine, University of the Ryukyus, Nishihara-cho 903-0215, Japan; [c]Graduate School of Frontier Biosciences, Osaka University, Suita 565-0871, Japan

ABSTRACT **The mammalian cell nucleus is a highly organized organelle that contains membrane-less structures referred to as nuclear bodies (NBs). Some NBs carry specific RNA types that play architectural roles in their formation. Here, we show two types of RNase-sensitive DBC1-containing NBs, DBC1 nuclear body (DNB) in HCT116 cells and Sam68 nuclear body (SNB) in HeLa cells, that exhibit phase-separated features and are constructed using RNA polymerase I or II transcripts in a cell type–specific manner. We identified additional protein components present in DNB by immunoprecipitation–mass spectrometry, some of which (DBC1 and heterogeneous nuclear ribonucleoprotein L [HNRNPL]) are required for DNB formation. The rescue experiment using the truncated HNRNPL mutants revealed that two RNA-binding domains and intrinsically disordered regions of HNRNPL play significant roles in DNB formation. All these domains of HNRNPL promote in vitro droplet formation, suggesting the need for multivalent interactions between HNRNPL and RNA as well as proteins in DNB formation.**

Monitoring Editor
Tom Misteli
National Institutes of Health, NCI

Received: Mar 16, 2021
Revised: Aug 24, 2021
Accepted: Aug 30, 2021

INTRODUCTION

Nuclei of higher eukaryotic cells are highly structured and possess multiple types of nuclear compartments called nuclear bodies (NBs). NBs contain various types of proteins and RNAs, and most of them function as the sites of synthesis, storage, and sequestration of specific RNAs, proteins, and ribonucleoprotein (RNP) complexes. In general, NBs likely serve to concentrate various regulatory factors that enhance specific biochemical reactions taking place in the NBs or suppress their activity out of the NBs (Staněk and Fox, 2017). For example, the nucleolus serves as the platform for both RNA polymerase I (RNAPI) transcription and ribosome biogenesis (Iarovaia *et al.*, 2019). Paraspeckles regulate gene expression through sequestration of the proteins, which further results in suppression of the activity of transcriptional regulation proteins (Prasanth *et al.*, 2005; Hirose *et al.*, 2014; Imamura *et al.*, 2014). The nuclear stress bodies (nSBs) regulate pre-mRNA splicing through an efficient phosphorylation of the sequestered serine- and arginine-rich pre-mRNA splicing factors (SRSFs) by CLK1, which is recruited during thermal stress recovery (Ninomiya *et al.*, 2020). Recent studies indicated that the intracellular liquid demixing (i.e., liquid–liquid phase separation), induced by multivalent interactions between intrinsically disordered regions (IDRs) in various RNA-binding proteins (RBPs), promotes the assembly of liquid droplet–like membrane-less organelles (Banani *et al.*, 2017; Uversky, 2017; Fox *et al.*, 2018). In some cases, RNA serves as a scaffold of these organelles in a way to interact with multiple RBPs that further promote multivalent interactions between the IDRs (Lin *et al.*, 2015; Shin and Brangwynne, 2017). It has been proposed that a class of long noncoding RNAs

This article was published online ahead of print in MBoC in Press (http://www.molbiolcell.org/cgi/doi/10.1091/mbc.E21-02-0081) on September 8, 2021.

*Address correspondence to: Taro Mannen (t-mannen@fc.ritsumei.ac.jp); Tetsuro Hirose (hirose@fbs.osaka-u.ac.jp).

Abbreviations used: Act D, actinomycin D; arcRNA, architectural RNA; COIL, coilin; DBC1, deleted in breast cancer 1; DNB, DBC1 nuclear body; DRB, 5,6-dichloro-1-β-D-ribofuranosylbenzimidazole; FBS, fetal bovine serum; GAPDH, glyceraldehyde-3-phosphate dehydrogenase; HD, hexanediol; HNRNP, heterogeneous nuclear ribonucleoprotein; IDR, intrinsically disordered regions; IGS, intergenic spacer; lncRNA, long noncoding RNA; MBP, maltose-binding protein; MS, mass spectrometry; NBs, nuclear bodies; nSBs, nuclear stress bodies; PR, proline-rich domain; RBP, RNA-binding proteins; RNAPI, RNA polymerase I; RNAPII, RNA polymerase II; RRM, RNA recognition motif; RT, room temperature; SNB, Sam68 nuclear body; SRSF, serine- and arginine-rich pre-mRNA splicing factors; TR, tetracycline repressor.

(lncRNAs) functions as the scaffold of specific NBs, thereby termed as architectural RNAs (arcRNAs) (Clemson *et al.*, 2009; Sasaki *et al.*, 2009; Sunwoo *et al.*, 2009; Chujo *et al.*, 2016; Yamazaki *et al.*, 2019). For example, NEAT1 arcRNA plays an essential role in paraspeckle assembly by the interaction with IDR-containing RBPs such as NONO and SFPQ (Sasaki *et al.*, 2009; Naganuma *et al.*, 2012; Hennig *et al.*, 2015; Yamazaki *et al.*, 2018). The nSBs are produced on HSATIII arcRNAs that recruit distinct sets of RBPs such as SRSF splicing regulators (Ninomiya *et al.*, 2020; Ninomiya and Hirose, 2020).

In our previous study, by screening of RNase-sensitive NBs, we have searched for novel NBs that are built on unidentified arcRNAs using the fluorescently tagged human cDNA library (Mannen *et al.*, 2016). Among the identified RNase-sensitive NBs, we found that Sam68 nuclear bodies (SNBs), which were detected at perinucleolar sites requiring RNA polymerase II (RNAPII) transcripts for their formation, are composed of two distinct RNase-sensitive substructures, Sam68 and DBC1, which are connected by the adaptor protein heterogeneous nuclear ribonucleoprotein L (HNRNPL) in HeLa cells. On the other hand, HCT116 cells form different RNase-sensitive NBs, which include DBC1 but not Sam68; therefore, we termed them DBC1 nuclear bodies (DNBs) (Mannen *et al.*, 2016). Except for DBC1, other RNA and protein components that constitute DNBs remain still unidentified.

In this study, we aimed to show that the DNB is an RNase-sensitive and liquid droplet–like NB that requires RNAPI transcripts. As the first step, we planned to identify the remaining protein components of DNB by immunoprecipitation–mass spectrometry (IP-MS) and to characterize each protein component, bearing in mind that DBC1 and HNRNPL are essential for DNB formation. A detailed domain dissection was predicted in order to examine whether the RNA-binding domains of HNRNPL, as well as the intrinsically disordered proline-rich domain (PR), can play significant roles in DNB formation and in vitro droplet formation.

RESULTS

Formation of DBC1 nuclear bodies requires both RNA and phase-separated structures

In HeLa cells, the SNBs are composed of both the Sam68 and DBC1 substructures, which are combined with a HNRNPL adaptor protein, whereas the DBC1 focal signals were detected as distinct foci lacking the Sam68 signals in HCT116 and NIH3T3 cells (Supplemental Figure S1A). The DNBs were unexceptionally detected as a single focus in HCT116 and NIH3T3 cells, whereas SNBs were detected as two foci in HeLa cells (Supplemental Figure S1B). We confirmed that the expression levels of the DBC1 and the Sam68 proteins were almost equivalent in these two cell lines (Supplemental Figure S1C), suggesting the presence of cell type–specific factor(s) in the formation of the SNB and the DNB. The DNBs found in HCT116 and NIH3T3 cells were sensitive to the RNase treatment, which was also observed for the DBC1 substructure in HeLa cells (Supplemental Figure S1D). In addition, we showed that both the DBC1 and the Sam68 substructures in HeLa cells were rapidly dispersed upon inhibition of RNAPII with 5,6-dichloro-1-β-D-ribofuranosylbenzimidazole (DRB) or a high-dose (0.3 μg/ml) of actinomycin D (Act D) (Figure 1A and Supplemental Figure S1E), indicating the necessity for RNAPII transcript(s) for the formation of both substructures (Chen *et al.*, 1999; Mannen *et al.*, 2016). We also found that these two substructures were poorly sensitive to the treatment with CX5461 or a low-dose (0.03 μg/ml) of Act D as RNAPI inhibitors in HeLa cells (Figure 1A and Supplemental Figure S1E). Unexpectedly, in HCT116 and NIH3T3 cells the DNBs were found to be highly sensitive to the treatment with CX5461 or a low-dose of Act D, but not to DRB (Figure 1A), suggesting the requirement for RNAPI transcripts for the DNB formation. RNAPI transcribes the ribosomal DNA unit, which produces a large precursor (47S) consisting of the 18S, 5.8S, and 28S rRNAs and intergenic spacer (IGS) regions (McStay and Grummt, 2008) (Supplemental Figure S2A). In response to various environmental stimuli, IGS regions produce lncRNAs called IGS RNAs, which sequester specific sets of proteins to assemble distinct phase-separated NBs called a nucleolar detention center (Audas *et al.*, 2012; Jacob *et al.*, 2013). We attempted to detect various IGS RNAs in DNBs; however, they were detectable only at perinucleolar sites, distinct from DNBs (Supplemental Figure S2B), suggesting that the IGS RNAs are neither localized in DNBs nor involved in DNB formation. These findings suggest that the DNBs in both HCT116 and NIH3T3 cells and the DBC1 substructures in SNBs of HeLa cells are likely different structures and may require distinct transcripts synthesized by other types of RNA polymerases.

Recent studies demonstrated that some NBs were in fact phase-separated ribonucleoprotein condensates formed by a multivalent interaction network of the NB components (Boeynaems *et al.*, 2018). To investigate whether DNBs and SNBs exhibit phase-separated features, HCT116 and HeLa cells were treated with 1,6-hexanediol (1,6-HD), which reportedly disintegrates the subsets of phase-separated subcellular structures in vivo by disrupting their multivalent hydrophobic interactions (Lin *et al.*, 2016; Cho *et al.*, 2018; Chong *et al.*, 2018; Sabari *et al.*, 2018; Yamazaki *et al.*, 2018). As shown in Figure 1B, the treatment with 1,6-HD in concentrations of 5% or 7.5% disrupted DNBs or SNBs, respectively. We also confirmed that Cajal bodies, which are phase-separated cellular structures detected with coilin (COIL) (Lin *et al.*, 2016), were also readily disintegrated in the same conditions (Figure 1B). On the other hand, 2,5-hexanediol (2,5-HD), which is known to have lower activity on the phase-separated structures, hardly affected the integrity of DNBs, SNBs, and Cajal bodies (Figure 1B). These findings suggest that DNBs in HCT116 cells and SNBs in HeLa cells exhibit characteristics similar to those of the other known phase-separated NBs.

HNRNPL and HNRNPK are novel DNB components

To gain insight into the assembly and maintenance of the DNB, we attempted to isolate the native complexes of DBC1 by IP. First, we established HCT116 cell lines stably expressing doxycycline-inducible DBC1-3xFLAG (HCT116/TR_DBC1-3xFLAG cells; Supplemental Figure S3A) and confirmed that the expressed DBC1-3xFLAG protein is promptly localized in the endogenous DNBs (Supplemental Figure S3B). To identify the proteins that interact with DBC1, an IP assay with anti-FLAG antibody was carried out using the DBC1-3xFLAG cell extracts either with or without RNase A treatment. This was followed by the analysis of the precipitated proteins with MS (Figure 2, A and B). The MS data showed that DBC1 coprecipitated with the mitochondrial chaperon HSPD1, HNRNPs HNRNPL, HNRNPK, PTBP1, and HNRNPA2B1, as well as with cytoplasmic poly(A)-binding protein PABPC1. Among these proteins, the coprecipitation of HNRNPL, HNRNPK, PTBP1, HNRNPA2B1, and PABPC1 was significantly decreased by the RNase A treatment (Figure 2B). We also confirmed both coprecipitation and RNase sensitivity of these proteins by Western blotting (Figure 2C and Supplemental Figure S4A). Among the coprecipitated proteins, we previously reported that PTBP1, which is known to be a marker of a distinct NB called the perinucleolar compartment, did not colocalize with DNBs in HCT116 cells (Mannen *et al.*, 2016). To confirm the localization of the other coprecipitated proteins in DNBs, we performed an immunofluorescence (IF) assay using the antibodies against the stated proteins (Figure 2D and Supplemental Figure S4B). Both HNRNPL

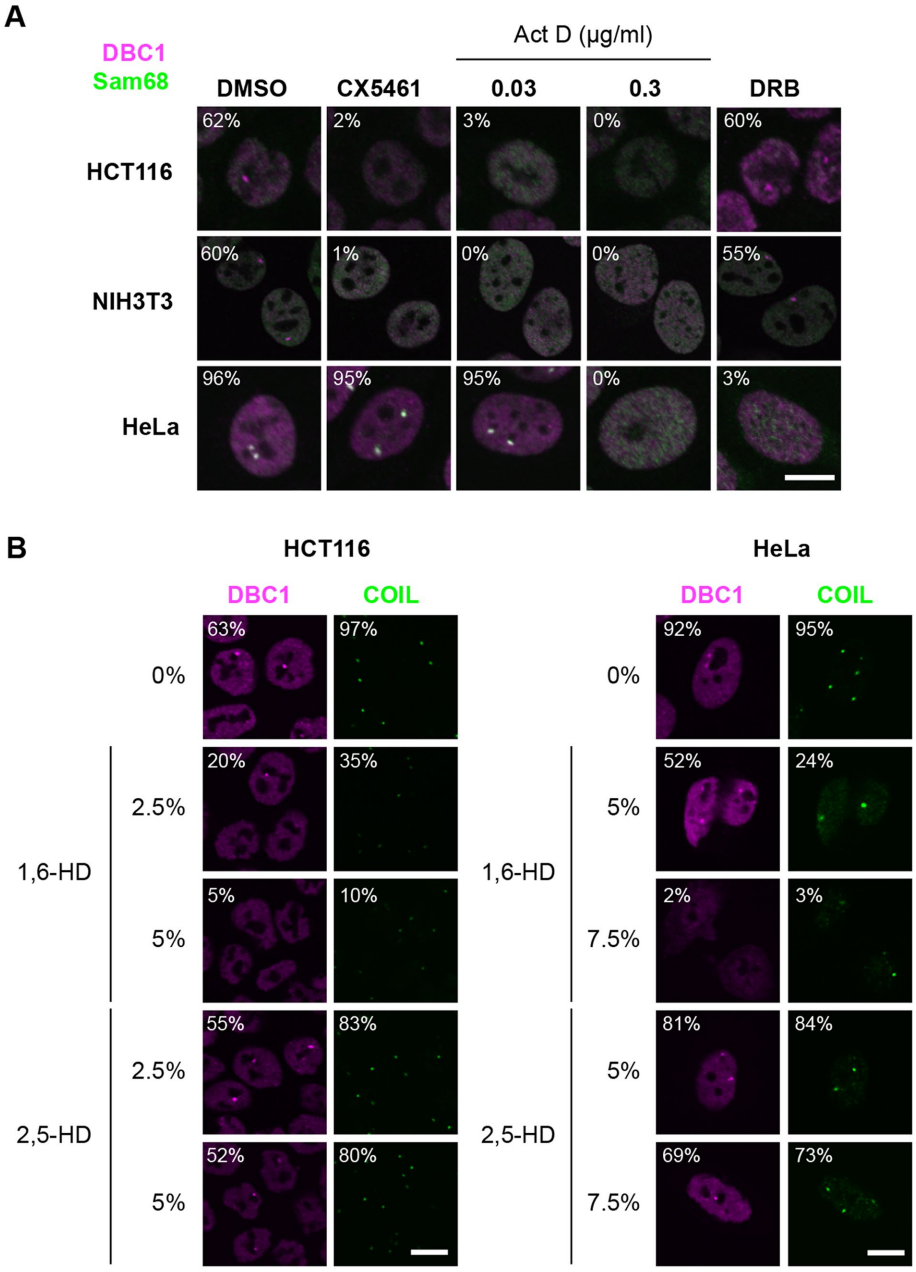

FIGURE 1: Features of the DNB. (A) DNB formation requires RNAPI transcription. IF analysis of both DBC1 (magenta) and Sam68 (green) was performed in either HCT116, NIH3T3, or HeLa cells treated with CX5461 (2 μM), Act D (0.03 and 0.3 μg/ml), or DRB (100 μM). The control cells were treated with DMSO. DNB (DBC1 signal) are detectable in HCT116 and NIH3T3 cells. SNB (DBC1 and Sam68 signals overlap) are detectable in HeLa cells. (B) IF analysis of DBC1 (magenta) and COIL (green) was performed in both HCT116 and HeLa cells treated with 0%–7.5% 1,6-HD or 2,5-HD. DNB and SNB were detected in DBC1. Cajal bodies were detected in COIL. Both nuclear body component signals dispersed upon 1,6-HD treatment. The cell populations (%) of summary NBs (DNB, SNB, and Cajal body) signals are shown in both A and B (>100 cells, $n = 5$). Bars, 10 μm.

and HNRNPK, but not HSPD1 and HNRNPA2B1, were clearly detected to be localized in DNB. The focal signals of all three DNB proteins (DBC1, HNRNPK, and HNRNPL) synchronously disappeared upon treatment with CX5461 in both HCT116 and NIH3T3 cells (Supplemental Figure S5, A and B). These data strongly support HNRNPL and HNRNPK being the additional DNB components in HCT116 and NIH3T3 cells.

DBC1 and HNRNPL are required for DNB formation

To investigate the mechanism of DNB assembly with the identified components, we performed a reciprocal depletion of each of the three DNB components (DBC1, HNRNPL, and HNRNPK) in HCT116 and NIH3T3 cells by an RNA interference (RNAi) approach (Figure 3, A and C). IF of the DNB components in the siRNA-treated cells revealed that the depletion of either DBC1 or HNRNPL resulted in DNBs' disappearance (see siDBC1 and siHNRNPL in Figure 3, B and D), while the depletion of HNRNPK hardly affected the DNBs' integrity (see siHNRNPK in Figure 3, B and D). These results indicate that DBC1 and HNRNPL are both required for the formation and maintenance of the DNB structure in HCT116 and NIH3T3 cells, although we cannot rule out the possibility that additional unidentified core factors are present in DNBs.

RRMs and PR of HNRNPL are both required for DNB formation

We previously showed that the S1L domain in the N-terminal region of DBC1 is required for its localization and RNA binding to the DNB in HCT116 cells (Mannen *et al.*, 2016). Here, we attempted to identify the functional domains of HNRNPL for DNB formation. We constructed a series of deletion mutants lacking the annotated domains in FLAG-tagged HNRNPL (Figure 4A), and the localization of each mutant was monitored by the anti-FLAG IF. We observed that the cell population in which DNBs with the FLAG signals were detected was markedly decreased in ΔRRM1, ΔRRM2, and ΔPR mutants (Supplemental Figure S6). In particular, ΔRRM2 was diffusely distributed throughout the nucleoplasm, while its small fraction was still detectable in the DNB (Supplemental Figure S6). We further investigated the rescue activity of each HNRNPL mutant for DNB formation in the HNRNPL-depleted cells. As shown in Figure 4B, WT, ΔGR, ΔRRM3, and ΔRRM4 had rescue activities that led to DNB formation in ~40% of cells; however, ΔRRM1 and ΔRRM2 attenuated the rescue activity to <20%. A co-IP assay of DBC1 with the FLAG-HNRNPL mutants revealed that neither ΔRRM1 nor ΔRRM2 of HNRNPL succeeded in interacting with DBC1 (Figure 4C), suggesting that the HNRNPL-DBC1 interaction via either RRM1 or RRM2 is required for the rescue activity of HNRNPL during DNB formation.

Meanwhile, ΔPR almost completely abolished rescue ability (Figure 4B). In contrast to ΔRRM1 and ΔRRM2, ΔPR was able to localize itself in DNBs (Supplemental Figure S6) and subsequently interacted with DBC1 but lacked rescue activity (Figure 4C). The PR has been reported as a part of the multiple IDRs, and as an intriguing

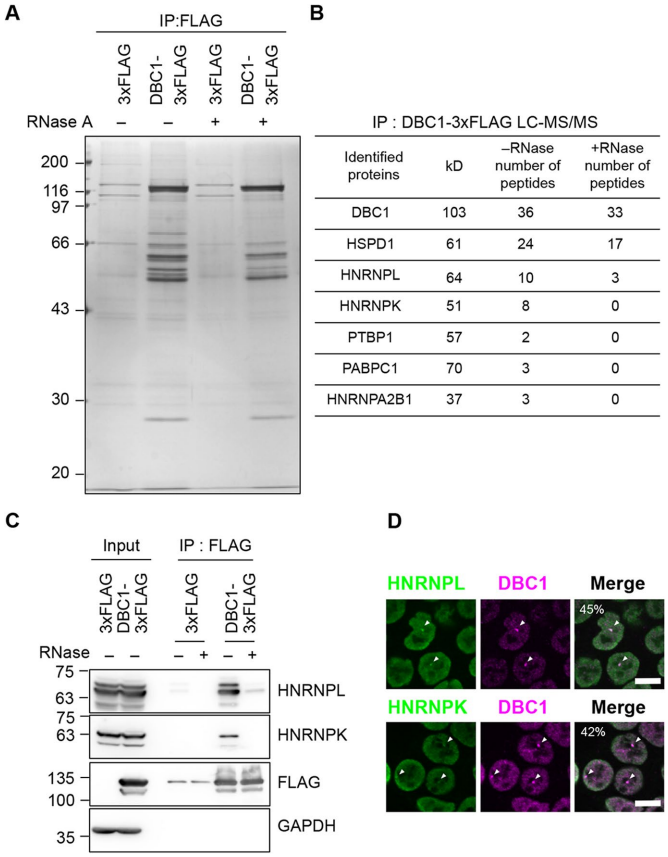

FIGURE 2: New components of DNB identified by IP-MS analysis. (A) Purification of DBC1-associated proteins from a stable cell line that express DBC1-3xFLAG and the effect of RNase treatment. Eluted proteins are confirmed by SDS–PAGE and silver stained. The molecular mass marker (kDa) is shown on the left. (B) Summary of proteins identified by mass spectrometric analysis with the expected molecular weights and the number of peptides. (C) IP of FLAG-tagged DBC1 to detect the interaction with HNRNPL and HNRNPK. Use of RNase treatment is indicated above the panels as "+" or "–." GAPDH (glyceraldehyde-3-phosphate dehydrogenase) was used as the input control. The molecular mass marker (kDa) is shown on the left. (D) IF analysis of DNB components. HNRNPL and HNRNPK colocalized in DNBs. The cell populations (%) in which the DNB signals were visible are shown in D (>100 cells, $n = 5$). Arrowheads indicate DNBs. Bars, 10 μm.

example, the PR of the phase-separated subcellular structures (N-WASP) is known to induce phase separation by interacting with multiple SH3 (Src homology 3) domains (Li *et al.*, 2012). The PR of HNRNPL was predicted to be disordered by IUPred2 (Supplemental Figure S7A). To examine whether the PR property is required for DNB formation, multiple proline residues in the PR were replaced with alanine residues to create two partial P-A mutants (PRmut1: four proline residues in the first part were altered; PRmut2: eight proline residues in the subsequent part were altered) and a full P-A mutant (PRmut3: 12 proline residues were altered; Figure 4A and Supplemental Figure S7B). All PR mutants were able to localize themselves to DNBs (Supplemental Figure S6). The plasmid rescue experiment showed that the PR mutants exhibited a significantly reduced ability to rescue the DNB formation in the HNRNPL-depleted cells (Figure 4B). However, the co-IP assay, which included the FLAG-PR mutants, revealed that they were still able to interact with DBC1 and the cotransfected Venus-tagged PR mutants themselves, but these interactions were disrupted by the RNase treatment (Figure 4C and Supplemental Figure S7C). These results suggested that the HNRNPL PR might contribute to DNB assembly through the RNA-bridged indirect interactions between HNRNPL and either DBC1 or HNRNPL.

RRMs and PR of HNRNPL promote in vitro droplet formation

Recent studies revealed that some NBs exhibited phase-separated liquid-like properties that are likely caused by demixing induced by the IDRs present in the RBP components (Banani *et al.*, 2017; Uversky, 2017; Fox *et al.*, 2018). To investigate whether the HNRNPL contributes to phase separation, we performed in vitro analysis using the recombinant HNRNPL protein fused with a maltose-binding protein (MBP-HNRNPL WT, a series of deletion mutants lacking the annotated domains, and PRmut3) (Supplemental Figure S8A). DNB concentrations of HNRNPL were estimated at 13.7 μM, and the in vitro protein concentration of HNRNPL was 3.3 μM (see *Materials and Methods*), suggesting that the HNRNPL concentration used in our in vitro experiment was within the level of HNRNPL in DNBs. We examined whether the TEV-cleaved HNRNPL proteins can form droplets under different salt conditions. The results were recorded by three different methods including sedimentation assay, turbidity assay, and microscopic observation (Supplemental Figure S8, B and C). In a sedimentation assay, TEV-cleaved HNRNPL WT, ΔGR, and PRmut3, was significantly decreased in the supernatant by reducing the NaCl concentrations, and ΔRRM3 and ΔRRM4 were nearly absent in the supernatant after centrifugation even at 150 mM NaCl, whereas ΔRRM1 and ΔRRM2 levels were unchanged by NaCl concentration and ΔPR declined slightly in 50 mM NaCl (Figure 5A and Supplemental Figure S8D). On the other hand, TEV-cleaved MBP was unaffected by different concentrations of NaCl (Figure 5A and Supplemental Figure S8D). In a turbidity assay, the turbidity of HNRNPL WT, ΔGR, ΔRRM3, ΔRRM4, and PRmut3 was decreased upon increasing salt concentration, while that of ΔRRM1, ΔRRM2, and ΔPR was significantly decreased in comparison to WT (Figure 5B and Supplemental Figure S8E). We also observed the turbid solutions of HNRNPL protein using microscopy (Figure 5C and Supplemental Figure S8F). HNRNPL WT, ΔGR, ΔRRM3, ΔRRM4, and PRmut3 formed dynamic liquid droplets, which increased in number by decreasing salt concentration (50–150 mM NaCl), whereas ΔRRM1, ΔRRM2, and ΔPR formed liquid droplets in 50 mM NaCl but failed in higher salt concentrations. In ΔRRM2, the formation of aggregates was detected at each concentration (Figure 5C), suggesting that this causes the reduction of the HNRNPL band in the sedimentation assay regardless of the salt concentration (Figure 5A). These results revealed that RRM1, RRM2, and PR of HNRNPL promote droplet formation in vitro.

Thus, our results indicate that the HNRNPL RRM1, RRM2, and PR contribute to both DNB assembly *in vivo* and droplet formation in vitro. These data suggest that the HNRNPL RRM1, RRM2, and PR-mediated phase separation would be, at least in part, the driving force of DNB assembly (Figure 6B).

DISCUSSION

In this study, we demonstrated that each of the two types of DBC1-containing NBs, DNB in HCT116 and NIH3T3 cells and SNB in HeLa cells, requires distinct RNA polymerase transcripts for its formation and maintenance. Considering the RNase-sensitive features of both DNB and SNB, these putative transcripts likely act as arcRNAs of the NBs (Figure 6A). Because the lncRNA expression tends to be cell type specific (Cabili *et al.*, 2011; Djebali *et al.*, 2012), cell type–specific

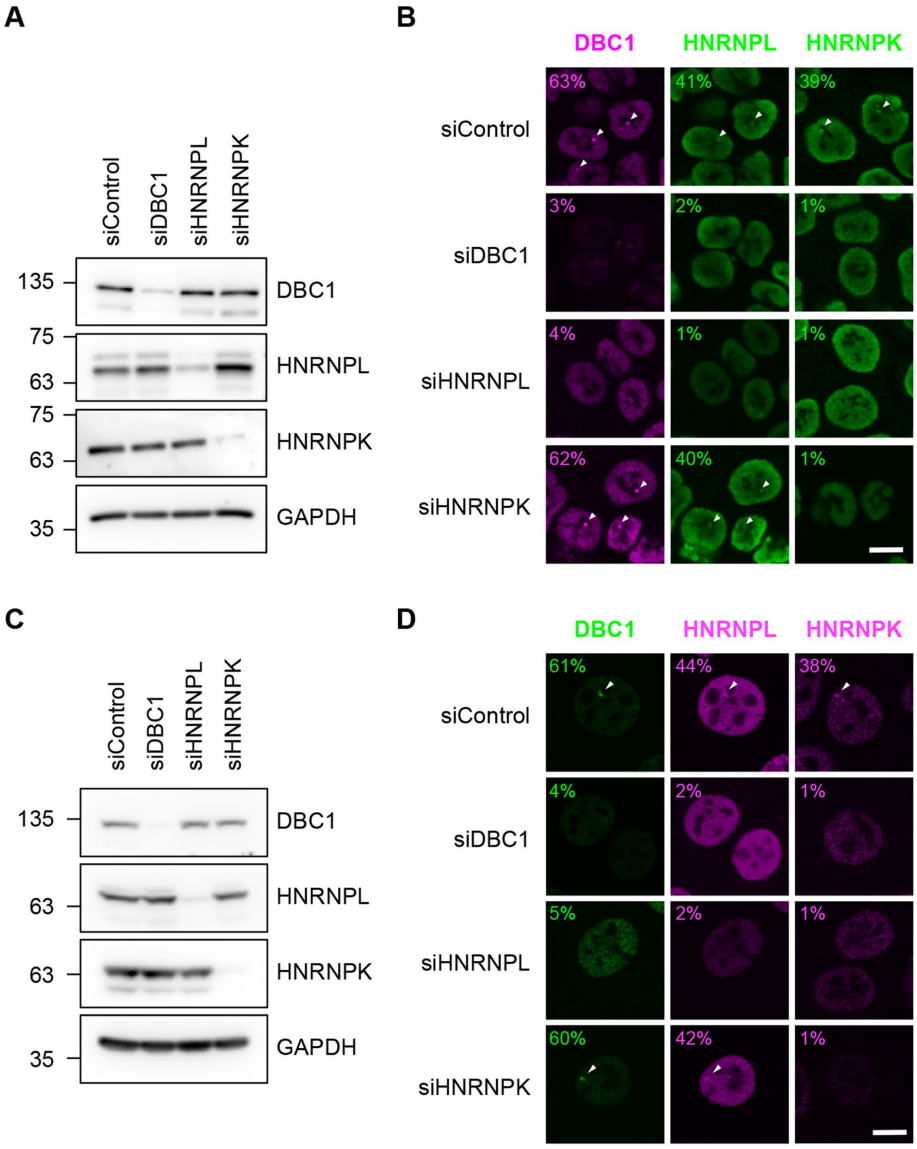

FIGURE 3: Identification of the essential DNB components. Three DNB components were reciprocally knocked down by RNAi in HCT116 and NIH3T3 cells. Both efficacy and specificity of knockdowns of each protein by RNAi were detected by Western blotting (A: HCT116 cells, C: NIH3T3 cells). The molecular mass marker (kDa) is shown on the left. Each protein was detected by IF (B: HCT116 cells, D: NIH3T3 cells). Arrowheads indicate DNBs. The cell populations (%) in which each protein signals is observed are shown in B and D (>100 cells, $n = 5$). Bar, 10 μm.

arcRNA may construct distinct DBC1-containing NBs. We carried out RNA fluorescence in situ hybridization (RNA-FISH) probes of IGS RNAs, RNAPI transcripts, and arcRNAs of the nucleolar detention center and found that they did not colocalize in DNBs (Supplemental Figure S2B), raising the possibility that an unidentified RNAPI transcript(s) form of the specific gene locus may be involved in the DNB formation. For example, de novo formation of both paraspeckles and nSBs is observed only at the transcription sites of NEAT1 and HSATIII lncRNAs (Mao *et al.*, 2011; Shevtsov and Dundr, 2011). In HCT116 and NIH3T3 cells, the DNB is detected as a single focus at the perinucleolar site (Supplemental Figure S1, A and B), which may support our hypothesis that a specific perinucleolar genomic locus transcribes arcRNA in the specific cell line.

Either DBC1 or HNRNPL knockdown resulted in disappearance of DNBs in HCT116 and NIH3T3 cells (Figure 3). In HeLa cells, on the other hand, DBC1 knockdown did not affect either the integrity of SNB or SNB localization of HNRNPL. Besides, HNRNPL knockdown resulted in the separation of SNBs into the Sam68 substructure and the DBC1 substructure (Mannen *et al.*, 2016). These results suggest that HNRNPL plays different roles in the formation of DNB compared with the formation of the DBC1 substructure in SNB (Figure 6A). The HNRNPL mutant lacking either RRM1 or RRM2 lost both the rescue activity for DNB formation and the interaction with DBC1 (Figure 4, B and C), suggesting that RRM1 and RRM2 cooperatively contribute to form the DNB through the interaction either with DBC1 or with arcRNA of the DNB (Figure 6B). On the other hand, HNRNPL mutants such as the ΔPR mutant and the PR substitution mutants (PRmut1-3) mostly lacked the rescue activity for DNB formation (Figure 4B), suggesting that PR of HNRNPL is required for DNB formation (Figure 6B). In addition, in vitro analysis of HNRNPL's RRM1, RRM2, and PR indicated the likelihood of droplet formation through a homomeric HNRNPL interaction, whereas PR substitution mutants (PRmut3) were unaffected for this ability (Figure 5). These results point out that the RRM1, RRM2, and PR of HNRNPL possibly contribute to the assembly of phase-separated DNBs through either a homomeric interaction with HNRNPL or a heteromeric interaction between HNRNPL and other DNB components. Our observation on the 1,6-HD sensitivity behavior of DNB also supports these arguments.

The biological roles of DNB remain elusive. It was reported that DBC1 directly interacts with SIRT1 to inhibit SIRT1 activity (Kim *et al.*, 2008; Zhao *et al.*, 2008). Indeed, our co-IP experiment detected the interaction of DBC1 with SIRT1; however, we failed to detect localization of SIRT1 in DNBs (Supplemental Figure S4, C and D), suggesting that DBC1 interacts with SIRT1 out of DNB and that DNB is not involved in the regulation of SIRT1 function. HNRNPL knockdown affects the early processing of 18S rRNAs, such as the increased abundance of 34S RNAs and the decreased abundance of both 26S and 18S-E RNAs (Tafforeau *et al.*, 2013). DNB including HNRNPL may regulate the optimal pre-rRNA processing events at the perinucleolus. To further understand the function of the DNB, it is of crucial importance to identify their arcRNAs. Functional analyses of arcRNAs will elucidate the mechanism underlying both the formation and the dynamics of DNBs as well as their biological functions. Detailed analyses of DNBs will reveal the nature of the mechanism underlying the functions of arcRNAs in the formation of arcRNA-dependent NBs.

MATERIALS AND METHODS

Request a protocol through *Bio-protocol*.

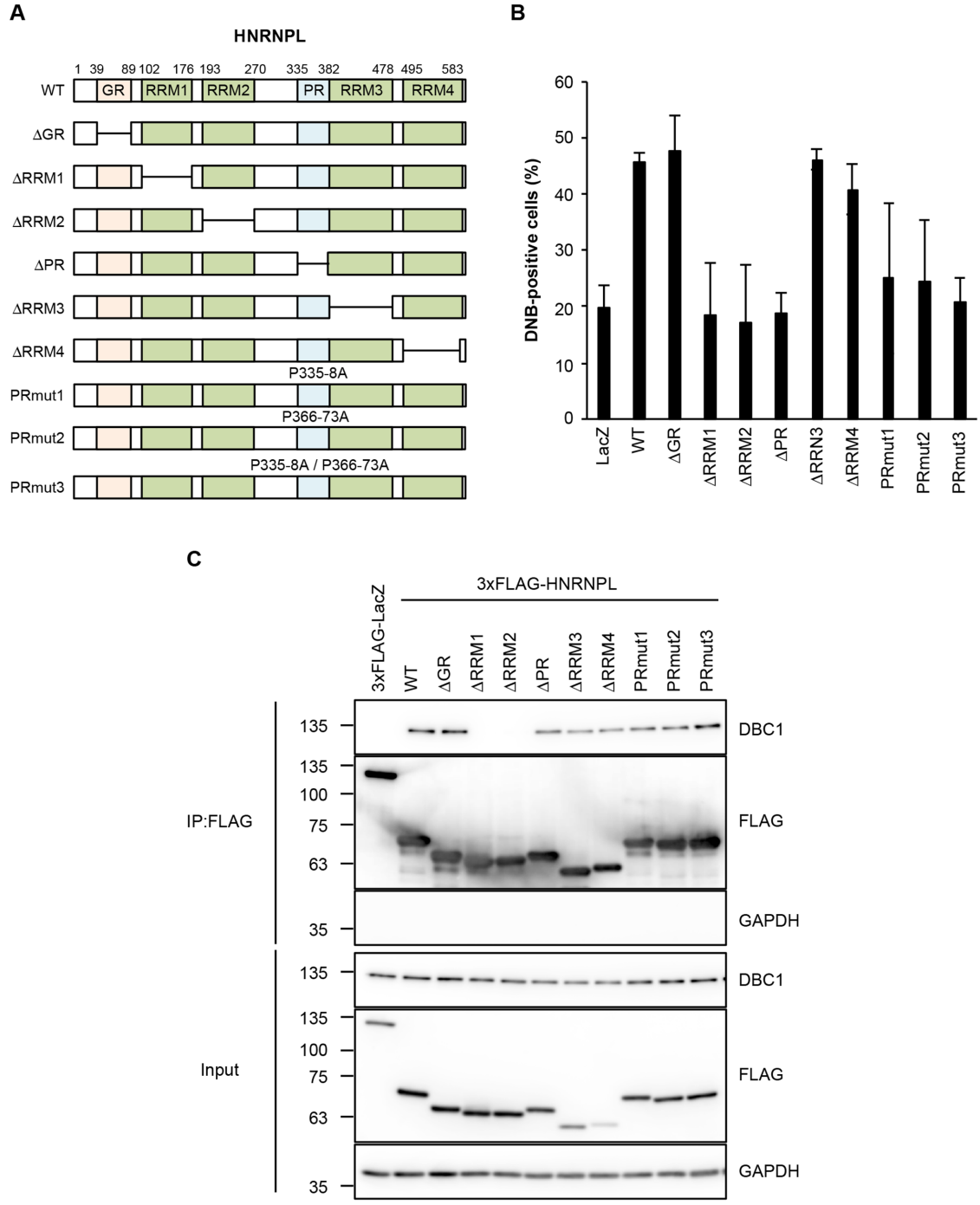

FIGURE 4: The RNA-binding domain and PR of HNRNPL are required for DNB formation. (A) Schematic presentation of both deletion mutants and point mutants of HNRNPL. For three point mutants (PRmut1, PRmut2, and PRmut3), the mutated residues are shown. (B) RRM1, RRM2, and PR are required for DNB formation. Rescue of the defect in DNB formation by the HNRNPL mutant constructs shown in A. The HNRNPL constructs were transfected into HCT116 cells in which the endogenous HNRNPL has been depleted by RNAi, and then DNB-positive cells (DBC1 foci–positive cells) were counted (>100 cells, ±SD, $n = 5$). As a negative control, the FLAG-LacZ plasmid was transfected (LacZ).
(C) Identification of the HNRNPL domains required for the interaction with DBC1. A series of FLAG-tagged HNRNPL mutants were immunoprecipitated, and coprecipitated DBC1 was detected by Western blotting. GAPDH denotes the input control. The molecular mass marker (kDa) is shown on the left.

Plasmid construction

The pcDNA5/FRT/TO-DBC1-3xFLAG plasmid was generated by inserting the PCR-amplified DBC1-3xFLAG sequence into the pcDNA5/FRT/TO vector (Thermo Fisher Scientific) between the *Eco*RV and *Xho*I sites. The pcDNA6/TR-IRES-puro plasmid was constructed by ligating the PCR-amplified sequence containing a pUC origin to the *TetR* gene of pcDNA6/TR (Thermo Fisher Scientific) with the segment of IRES to the puromycin-resistance gene of pCAGGS-FLPe (Gene Bridges) between the *Eco*RI and *Pst*I sites. The HNRNPL-deletion mutants were constructed as described

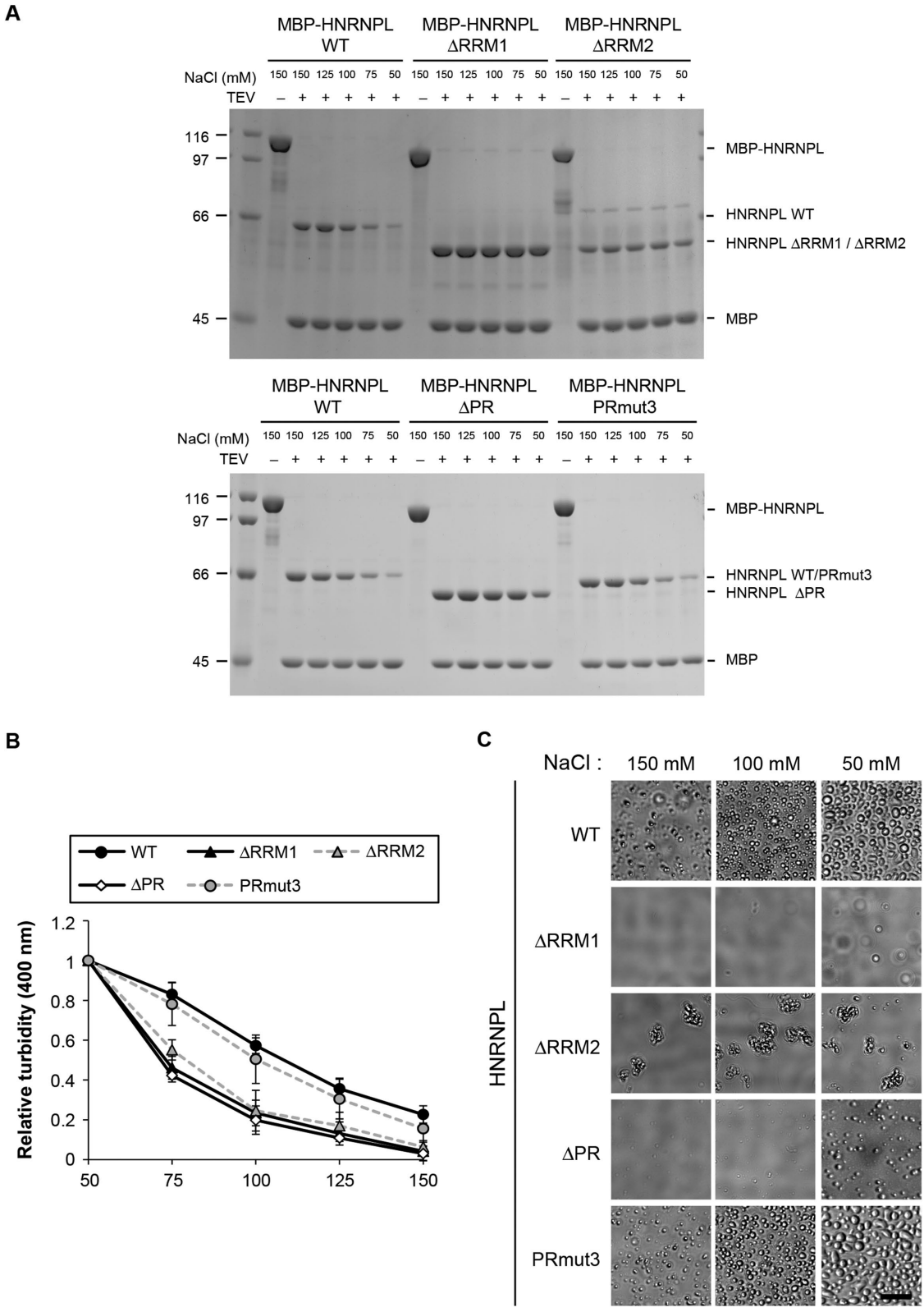

FIGURE 5: The RRM and PR of HNRNPL contribute to phase separation. (A) Sedimentation assay with the indicated salt concentrations of HNRNPL. The presence or the absence of TEV protease is shown above the panel ("+" or "–"). The molecular mass marker (kDa) is shown on the left. (B) Turbidity assay with the indicated NaCl concentrations of HNRNPL. Mean of five independent experiments, ±SD. (C) Imaging of the indicated salt concentrations of HNRNPL. Bar, 20 μm.

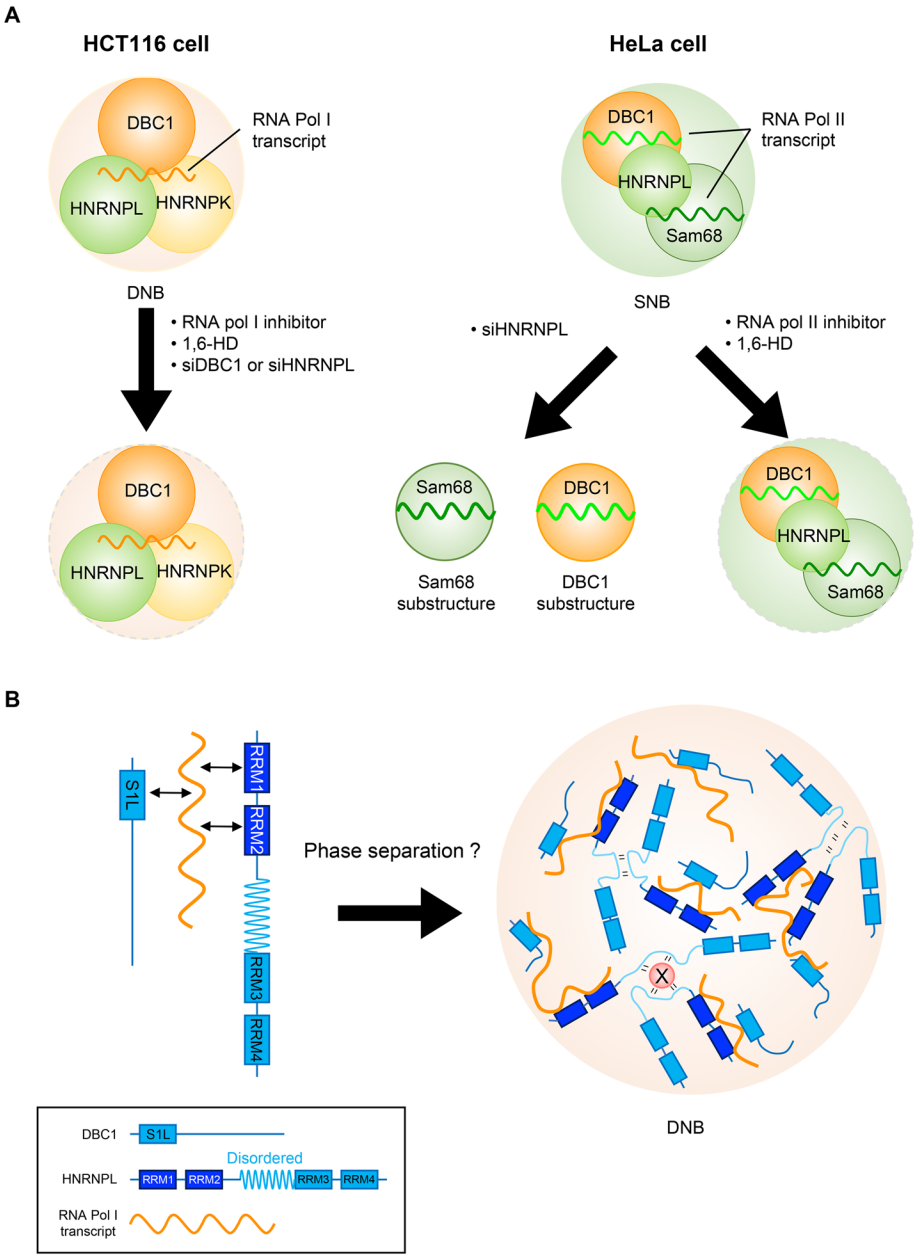

FIGURE 6: Model of the DNB architecture in HCT116 cells. (A) The DNB and SNB are constructed by distinct RNA polymerase transcripts (orange wavy line denotes the RNAPI transcript, while both yellow-green and green wavy lines represent RNAPII transcripts). The DNB disappears under certain conditions, including RNAPI inhibitor treatment, 1,6-HD treatment, and knockdown of either DBC1 or HNRNPL (siDBC1 or siHNRNPL) in HCT116. The SNB is separated into two substructures (Sam68 and DBC1) upon knockdown of HNRNPL (siHNRNPL) in HeLa cells. The SNB disappears under certain conditions, including RNAPII inhibitor treatment and 1,6-HD treatment in HeLa cells. (B) Molecular interactions within DNB. DBC1 interacts with the putative arcRNA through the S1-like RNA-binding domain (S1L). HNRNPL interacts with the putative arcRNA through either RRM1 or RRM2. The PR (disordered region; light blue wavy line) of HNRNPL may induce DNB assembly through the phase separation. X represents a hypothetical protein.

previously (Mannen *et al.*, 2016). The mutated residues of HNRNPL PRmut1 were P335A, P336A, P337A, and P338A, while those of HNRNPL PRmut2 were P366A, P367A, P368A, P369A, P370A, P371A, P372A, and P373A, and those of HNRNPL PRmut3 were P335A, P336A, P337A, P338A, P366A, P367A, P368A, P369A, P370A, P371A, P372A, and P373A. The HNRNPL PR mutants were generated by site-directed mutagenesis using PCR. The pMAL_TEV-HNRNPL plasmid was generated by inserting the PCR-amplified HNRNPL sequence into the pMAL_TEV vector (Yoshizawa *et al.*, 2018) between the *Hin*dIII and *Bam*HI sites. The primers used are listed in Supplemental Table S1.

Cell culture

We generated HCT116/TR_DBC1-3xFLAG cells using the Flp-In System (Thermo Fisher Scientific). First, we generated the doxycycline-induced HCT116/FRT stable cell lines, HCT116/FRT/TR, that express the tetracycline repressor (TR) from pcDNA6/TR-IRES-puro. The pcDNA6/TR-IRES-puro plasmids were transfected using Lipofectamine 3000 (Thermo Fisher Scientific) into the HCT116/FRT cells (Satoh *et al.*, 2014) and selected with 2 μg/ml puromycin, and single clones of HCT116/FRT/TR cells were isolated. HCT116/TR_DBC1-3xFLAG cells were prepared using the isolated HCT116/FRT/TR by the Flp-In System and cultured at 37°C with 5% CO_2 in DMEM/10% fetal bovine serum (FBS), supplemented with 2 μg/ml puromycin and 200 μg/ml hygromycin B. HCT116, NIH3T3, and HeLa cells were cultured in DMEM/10% FBS at 37°C with 5% CO_2. The cells were treated with CX5461 (2 μM, AdooQ Bioscience), actinomycin D (0.03 μg/ml or 0.3 μg/ml, Wako) and DRB (100 μM, TCI) for 4 h or 1,6-HD and 2,5-HD (2.5%, 5% or 7.5%, Sigma-Aldrich) for 5 min, respectively.

RNase treatment of cells

The RNase treatment was performed as described previously (Mannen *et al.*, 2016). Briefly, the cells were seeded onto round, 12-mm-diameter coverslips of 24-well plates, rinsed in phosphate-buffered saline (PBS), and then rinsed in a permeabilization buffer (20 mM Tris-HCl, pH 7.4, 5 mM $MgCl_2$, 0.5 mM EGTA (ethylene glycol tetraacetic acid), and cOmplete, Mini, EDTA-free protease inhibitor cocktail [Sigma-Aldrich]). Subsequently, cells were permeabilized for 10 min at room temperature (RT) in the permeabilization buffer containing 2% Tween-20 and then rinsed once with the sole permeabilization buffer. The permeabilized cells were incubated with RNase A (Nacalai Tesque; 1 μg/ml prepared in PBS) for 20 min at RT. After the RNase treatment, cells were rinsed with PBS and fixed with 4% paraformaldehyde prepared in PBS at RT for 10 min. The fixed cells were permeabilized with 0.5% Triton X-100 prepared in PBS for 15 min, rinsed, and blocked with 1% bovine serum albumin (BSA) prepared in PBS containing 0.1% Tween-20 (PBST) for 1 h. The slides were

incubated at 4°C overnight with primary antibodies (diluted in PBST containing 1% BSA) against specific proteins. Unbound antibodies were removed by three 10-min washes with PBST. The slides were then incubated with Alexa-conjugated secondary antibodies (Thermo Fisher Scientific) for 1 h at RT, washed, and mounted with Fluoro-KEEPER Antifade Reagent (Nacalai Tesque). Immunostained cells were examined using a confocal laser scanning microscope (FV1000D; Olympus). The antibodies used are listed in Supplemental Table S1.

Plasmid transfection

For microscopic observation, cells were seeded onto round, 12-mm-diameter coverslips of 24-well plates and transfected with plasmids using Lipofectamine 3000 (Thermo Fisher Scientific) according to the manufacturer's instructions. The cells were usually fixed 24 h after transfection. For both small interfering RNA (siRNA) transfection and plasmid rescue experiments, cells were seeded onto round, 12-mm-diameter coverslips of 24-well plates and transfected with siRNA using Lipofectamine RNAi MAX (Thermo Fisher Scientific) according to the manufacturer's instructions. Twenty-four hours after siRNA transfection, cells were transfected with plasmids using Lipofectamine 3000 (Thermo Fisher Scientific) according to the manufacturer's instructions. The cells were usually fixed 24 h after transfection.

RNA interference

Stealth siRNAs were purchased from Thermo Fisher Scientific. Cells were grown in six-well plates and transfected with siRNAs (33 nM, final concentration) using the Lipofectamine RNAi MAX reagent (Thermo Fisher Scientific) according to the manufacturer's instructions. After 24 h, the cells were trypsinized and seeded into six-well plates for the preparation of proteins or onto round, 12-mm-diameter coverslips of 24-well plates for the immunocytochemical experiments. The cells were cultured for 24 h before harvesting. The si-Control was purchased from Thermo Fisher Scientific (12935300). The siRNAs used are listed in Supplemental Table S1.

RNA-FISH

The RNA probes were synthesized using either T7 or SP6 RNA polymerase using a digoxigenin (DIG) RNA labeling kit (Roche). Linearized plasmids (1 µg) containing an IGS fragment were used as templates for transcription. RNA-FISH was performed as described previously (Mito *et al.*, 2016). Briefly, the cells were seeded onto a multichamber culture slide, washed with PBS, and fixed with 4% paraformaldehyde prepared in PBS at RT for 10 min. The fixed cells were treated with 0.2 N HCl for 20 min and then with 3 mg/ml proteinase K at 37°C for 5 min. The slides were incubated with a prehybridization solution (2× SSC (saline sodium citrate), 1× Denhardt's solution, 50% formamide, 10 mM EDTA, pH 8.0, 100 µg/ml yeast tRNA, and 0.01% Tween-20) at 55°C for 2 h. The prehybridized slides were then incubated with a hybridization solution (made of the prehybridization solution supplemented with 5% dextran sulfate and 2 µg/ml DIG-labeled RNA probe) at 55°C for 16 h. After hybridization, the slides were washed twice with a preheated wash buffer (2× SSC, 50% formamide, and 0.01% Tween-20) at 55°C for 30 min, while the excessive RNA probes were digested by incubation with 10 µg/ml RNase A prepared in NTET buffer (10 mM Tris-HCl, pH 8.0, 1 mM EDTA, 500 mM NaCl, and 0.1% Tween-20) at 37°C for 1 h. The slides were then washed once with buffer A (2× SSC and 0.01% Tween-20) at 55°C for 30 min and twice with buffer B (0.1× SSC and 0.01% Tween-20) at 55°C for 30 min. For detection, the slides were washed with Tris-buffered saline containing 0.1% Tween-20 (TBST), incubated with a blocking solution (3% BSA prepared in TBST) at RT for 1 h, and subsequently incubated with anti-DIG antibodies diluted in the blocking solution at 4°C overnight. Unbound antibodies were removed by three 15-min washes in TBST. The slides were then incubated with Alexa-conjugated secondary antibodies diluted in the blocking solution for 1 h at RT. After washing, the slides were mounted with Vectashield (Vector Laboratories) containing 4′,6-diamidino-2-phenylindole (DAPI). Fluorescence images were visualized at RT on a microscope (FV1000D; Olympus). The primers and antibodies used are listed in Supplemental Table S1.

Immunofluorescence

Cells were seeded onto round, 12-mm-diameter coverslips and fixed with 4% paraformaldehyde prepared in PBS at RT for 10 min. The fixed cells were permeabilized with 0.5% Triton X-100 prepared in PBS for 15 min, rinsed, and blocked with 1% BSA prepared in PBS containing 0.1% Tween-20 (PBST) for 1 h. The slides were incubated at 4°C overnight with primary antibodies (diluted in PBST containing 1% BSA) against specific proteins. Unbound antibodies were removed by three 10-min washes with PBST. The slides were then incubated with Alexa-conjugated secondary antibodies for 1 h at RT, washed, and mounted with Fluoro-KEEPER Antifade Reagent (Nacalai Tesque). Immunostained cells were examined using a confocal laser scanning microscope (FV1000D; Olympus). The antibodies used are listed in Supplemental Table S1.

Immunoblotting

Cells were lysed in a lysis buffer (50 mM Tris-HCl, pH 8.0, 150 mM NaCl, 0.5% IGEPAL CA630, 1 mM dithiothreitol [DTT], and cOmplete EDTA-free protease inhibitor [Sigma-Aldrich]) and then disrupted by three pulses of sonication for 10 s. The cell extracts were cleared by centrifugation, and the protein concentration was determined using the Bradford method. A one-fifth volume of the 5× SDS sample buffer was added, and the samples were heated before the SDS–PAGE separation. After fractionation, the proteins were transferred to Immobilon-P Transfer membranes (Merck) by electroblotting. The antibodies used are listed in Supplemental Table S1.

Immunoprecipitation

HCT116 cells were suspended in the lysis buffer for 10 min on ice and then disrupted by three pulses of sonication for 10 s. The resultant cell extracts were cleared by centrifugation at 20,400 × *g* for 10 min. The supernatant containing the HCT116 cells' extract was mixed with the anti-DYKDDDDK magnetic agarose (Thermo Fisher Scientific) and rotated at 4°C overnight. The beads were finally washed five times with lysis buffer. For the RNase treatment, the beads were washed three times and treated with RNase A (1 µg/ml) at 4˚C for 3 h or were left untreated. The beads were then washed two times with the lysis buffer. The IP samples were eluted from the beads by 500 µg/ml 3xFLAG peptide (Protein Ark) at 4°C for 1 h.

Mass spectrometric analysis

Peptide mixtures for mass spectrometric analysis were prepared as described previously (Kanayama *et al.*, 2017). Proteins in IP samples were precipitated with 10% trichloroacetic acid, resuspended in 20 µl 100 mM Tris-HCl buffer, pH 8.8, containing 6 M urea, and reduced by adding 2 µl 50 mM Tris-(2-carboxyethyl) phosphine and incubating at 60°C for 1 h. The generated free sulfhydryl groups were alkylated with 1 µl 20 mM methyl methanethiosulfonate by incubation at RT for 10 min. Proteins were digested by 1 µg of lysyl endopeptidase (Wako) at 37°C overnight. The resulting peptide mixtures were desalted with C18 Empore Disks (3M) and subjected to Liquid Chromatograph (LC)-MS/MS analysis as described earlier

(Tohsato *et al.*, 2012). The peptides were loaded on a frit-less Mightysil C18 column, washed with 2% acetonitrile in 0.1% formic acid, and eluted using the DiNa AI automatic system (KYA TECH) at a flow rate of 0.2 µl/min and the following elution gradient: 0%–50% solvent B (80% acetonitrile in 0.1% formic acid) in solvent A (2% acetonitrile in 0.1% formic acid) from 0 to the 195th min, 50%–100% solvent B in solvent A from the 195th to the 210th min, and 100% solvent B from the 210th to the 220th min. MS/MS analysis was performed by using a Q-TOF hybrid mass spectrometer (QSTAR Elite; AB Sciex). Protein identification was performed using ProteinPilot software 2.0 (AB Sciex) against the human UniProt database (version 2015_11) as described by Tohsato *et al.* (2012).

Estimation of the concentrations of HNRNPL in DNB

The cellular abundance levels of proteins, measured via MS-based quantitative proteomics studies, were obtained from the PaxDb (Wang *et al.*, 2015). The cell line–integrated abundance values retrieved from PaxDb were converted into concentrations using the following formula:

$$C = (k \times A) / N_A$$

(Milo, 2013), where $k \approx 3 \times 10^6$ proteins/fl, the Avogadro constant $N_A = 6.02 \times 10^{23}$ molecules/mol, and A is the abundance. The intracellular concentration of HNRNPL was estimated at 2.0 µM. Our cell fractionation experiment determined that the intracellular distribution of HNRNPL in nuclei and cytoplasm was 4:1 (Supplemental Figure S9). In addition, the nuclear-to-cytoplasmic volume (N/C) ratio of HCT116 was approximately 0.18 (Ganguly *et al.*, 2016). Consequently, the nuclear and cytoplasmic concentrations of HNRNPL were estimated to be 5.5 and 1.4 µM, respectively. The nucleoplasm and DNB volumes as well as the proportion of HNRNPL protein present within the DNB were estimated from the IF intensity profile over different Z positions (Z-stack) using cellSens Dimension software (Olympus). The ratio of nucleoplasm volume to DNB volume was 629:1, whereas the ratio of the proportion of HNRNPL protein present in the nucleoplasm to that in the DNB was 0.4:1.0. Consequently, the nucleoplasmic and DNB concentrations of HNRNPL were estimated at 5.5 and 13.7 µM, respectively.

Recombinant protein expression and purification

All recombinant proteins were expressed individually in Rosetta 2 (DE3) *Escherichia coli* cells (Novagen; induced with 0.5 mM isopropyl-β-D-1-thiogalactoside [IPTG] for 16 h at 18°C). Bacteria expressing MBP-HNRNPL proteins were lysed using a cell homogenizer (QSonica) in a lysis buffer (50 mM Tris-HCl, pH 7.4, 500 mM NaCl, 10% [vol/vol] glycerol, 2 mM DTT). MBP-HNRNPL proteins were purified by affinity chromatography using amylose resin (NEB), eluted with the lysis buffer containing 20 mM maltose, and purified by gel filtration chromatography using a HiLoad 16/600 Superdex 200 pg column (GE Healthcare). The purified proteins were freshly frozen in liquid nitrogen and stored at −80°C. Protein concentrations were determined by absorbance at 280 nm using their extinction coefficients predicted by the ProtParam tool. MBP-HNRNPL proteins (10 µM) (dissolved in a buffer containing 50 mM Tris-HCl, pH 7.4, 150 mM NaCl, 10% [vol/vol] glycerol, 2 mM DTT) were treated with Tobacco Etch Virus (TEV) protease (Sigma-Aldrich; 25 µg/ml TEV, final concentration) in reaction volumes of 400 µl for 3 h at 30°C.

Sedimentation assay

For sedimentation analysis of HNRNPL, 10 µM purified and TEV-treated HNRNPL and NaCl were mixed into a buffer containing 50 mM Tris-HCl, pH 7.4, 10% (vol/vol) glycerol, and 2 mM DTT (50, 75, 100, 125, or 150 mM, final salt concentration). HNRNPL was subsequently diluted to a final concentration of 3.3 µM. Dilutions of HNRNPL supplemented with salt in the indicated concentrations were centrifuged for 10 min at 20,400 × *g* at 25°C. The supernatant was separated by SDS–PAGE and stained with Coomassie Brilliant Blue.

Turbidity assay

For turbidity analysis of HNRNPL, the absorbance of 3.3 µM TEV-treated HNRNPL proteins at the indicated final salt concentrations of 50, 75, 100, 125, or 150 mM (dissolved in a buffer containing 50 mM Tris-HCl, pH 7.4, 10% [vol/vol] glycerol, and 2 mM DTT) was measured at 400 nm using a SH-1000 plate reader (CORONA ELECTRIC). Values were normalized to a 50 mM NaCl concentration of HNRNPL to determine the relative turbidity value.

Imaging of the turbid HNRNPL solution

For imaging experiments, 3.3 µM TEV-treated HNRNPL proteins at the indicated final salt concentrations of 50, 75, 100, 125, or 150 mM (dissolved in a buffer containing 50 mM Tris-HCl, pH 7.4, 10% [vol/vol] glycerol, 2 mM DTT) were dropped onto individual wells of 96-well Optical-Bottom Plates (Thermo Fisher Scientific) and observed by microscope (Eclipse Ti2, Nikon) at RT.

ACKNOWLEDGMENTS

We thank Y. Shinjo and T. Kato (Olympus marketing) for their assistance with fluorescence quantification. This research was supported by grants from the Ministry of Education, Culture, Sports, Science, and Technology of Japan (to T.M. [17K15112 and 20K06493] and to T. Hirose [20H00448 and 20H05377]), JST CREST (to T. Hirose [JPMJCR20E6]), a Basic Science research project of the Sumitomo Foundation (to T.M.), the Joint Research Program of the Institute for Genetic Medicine, Hokkaido University (to T.M.), the MEXT-Supported Program for the Strategic Research Foundation at Private Universities (to T.M. and T. Hayano), and the Takeda Science Foundation (to T.M. and T. Hayano).

REFERENCES

Audas TE, Jacob MD, Lee S (2012). Immobilization of proteins in the nucleolus by ribosomal intergenic spacer noncoding RNA. Mol Cell 45, 147–157.

Banani SF, Lee HO, Hyman AA, Rosen MK (2017). Biomolecular condensates: organizers of cellular biochemistry. Nat Rev Mol Cell Biol 18, 285–298.

Boeynaems S, Alberti S, Fawzi NL, Mittag T, Polymenidou M, Rousseau F, Schymkowitz J, Shorter J, Wolozin B, Van Den Bosch L, *et al.* (2018). Protein phase separation: a new phase in cell biology. Trends Cell Biol 28, 420–435.

Cabili MN, Trapnell C, Goff L, Koziol M, Tazon-Vega B, Regev A, Rinn JL (2011). Integrative annotation of human large intergenic noncoding RNAs reveals global properties and specific subclasses. Genes Dev 25, 1915–1927.

Chen T, Boisvert FM, Bazett-Jones DP, Richard S (1999). A role for the GSG domain in localizing Sam68 to novel nuclear structures in cancer cell lines. Mol Biol Cell 10, 3015–3033.

Cho WK, Spille JH, Hecht M, Lee C, Li C, Grube V, Cisse II (2018). Mediator and RNA polymerase II clusters associate in transcription-dependent condensates. Science 361, 412–415.

Chong S, Dugast-Darzacq C, Liu Z, Dong P, Dailey GM, Cattoglio C, Heckert A, Banala S, Lavis L, Darzacq X, Tjian R (2018). Imaging dynamic and selective low-complexity domain interactions that control gene transcription. Science 361, eaar2555.

Chujo T, Yamazaki T, Hirose T (2016). Architectural RNAs (arcRNAs): a class of long noncoding RNAs that function as the scaffold of nuclear bodies. Biochim Biophys Acta 1859, 139–146.

Clemson CM, Hutchinson JN, Sara SA, Ensminger AW, Fox AH, Chess A, Lawrence JB (2009). An architectural role for a nuclear noncoding RNA: NEAT1 RNA is essential for the structure of paraspeckles. Mol Cell 33, 717–726.

Djebali S, Davis CA, Merkel A, Dobin A, Lassmann T, Mortazavi A, Tanzer A, Lagarde J, Lin W, Schlesinger F, *et al*. (2012). Landscape of transcription in human cells. Nature 489, 101–108.

Fox AH, Nakagawa S, Hirose T, Bond CS (2018). Paraspeckles: where long noncoding RNA meets phase separation. Trends Biochem Sci 43, 124–135.

Ganguly A, Bhattacharjee C, Bhave M, Kailaje V, Jain BK, Sengupta I, Rangarajan A, Bhattacharyya D (2016). Perturbation of nucleo-cytoplasmic transport affects size of nucleus and nucleolus in human cells. FEBS Lett 590, 631–643.

Hennig S, Kong G, Mannen T, Sadowska A, Kobelke S, Blythe A, Knott GJ, Iyer KS, Ho D, Newcombe EA, *et al*. (2015). Prion-like domains in RNA binding proteins are essential for building subnuclear paraspeckles. J Cell Biol 210, 529–539.

Hirose T, Virnicchi G, Tanigawa A, Naganuma T, Li R, Kimura H, Yokoi T, Nakagawa S, Bénard M, Fox AH, *et al*. (2014). NEAT1 long noncoding RNA regulates transcription via protein sequestration within subnuclear bodies. Mol Biol Cell 25, 169–183.

Iarovaia OV, Minina EP, Sheval EV, Onichtchouk D, Dokudovskaya S, Razin SV, Vassetzky YS (2019). Nucleolus: a central hub for nuclear functions. Trends Cell Biol 29, 647–659.

Imamura K, Imamachi N, Akizuki G, Kumakura M, Kawaguchi A, Nagata K, Kato A, Kawaguchi Y, Sato H, Yoneda M, *et al*. (2014). Long noncoding RNA NEAT1-dependent SFPQ relocation from promoter region to paraspeckle mediates IL8 expression upon immune stimuli. Mol Cell 53, 393–406.

Jacob MD, Audas TE, Uniacke J, Trinkle-Mulcahy L, Lee S (2013). Environmental cues induce a long noncoding RNA-dependent remodeling of the nucleolus. Mol Biol Cell 24, 2943–2953.

Kanayama M, Hayano T, Koebis M, Maeda T, Tabe Y, Horie S, Aiba A (2017). Hyperactive mTOR induces neuroendocrine differentiation in prostate cancer cell with concurrent up-regulation of IRF1. Prostate 77, 1489–1498.

Kim JE, Chen J, Lou Z (2008). DBC1 is a negative regulator of SIRT1. Nature 451, 583–586.

Li P, Banjade S, Cheng HC, Kim S, Chen B, Guo L, Llaguno M, Hollingsworth JV, King DS, Banani SF, *et al*. (2012). Phase transitions in the assembly of multivalent signalling proteins. Nature 483, 336–340.

Lin Y, Mori E, Kato M, Xiang S, Wu L, Kwon I, McKnight SL (2016). Toxic PR poly-dipeptides encoded by the C9orf72 repeat expansion target LC domain polymers. Cell 167, 789–802.

Lin Y, Protter DS, Rosen MK, Parker R (2015). Formation and maturation of phase-separated liquid droplets by RNA-binding proteins. Mol Cell 60, 208–219.

Mannen T, Yamashita S, Tomita K, Goshima N, Hirose T (2016). The Sam68 nuclear body is composed of two RNase-sensitive substructures joined by the adaptor HNRNPL. J Cell Biol 214, 45–59.

Mao YS, Sunwoo H, Zhang B, Spector DL (2011). Direct visualization of the co-transcriptional assembly of a nuclear body by noncoding RNAs. Nat Cell Biol 13, 95–101.

McStay B, Grummt I (2008). The epigenetics of rRNA genes: from molecular to chromosome biology. Annu Rev Cell Dev Biol 24, 131–157.

Milo R (2013). What is the total number of protein molecules per cell volume? A call to rethink some published values. Bioessays 35, 1050–1055.

Mito M, Kawaguchi T, Hirose T, Nakagawa S (2016). Simultaneous multicolor detection of RNA and proteins using super-resolution microscopy. Methods 98, 158–165.

Naganuma T, Nakagawa S, Tanigawa A, Sasaki YF, Goshima N, Hirose T (2012). Alternative 3′-end processing of long noncoding RNA initiates construction of nuclear paraspeckles. EMBO J 31, 4020–4034.

Ninomiya K, Adachi S, Natsume T, Iwakiri J, Terai G, Asai K, Hirose T (2020). LncRNA-dependent nuclear stress bodies promote intron retention through SR protein phosphorylation. EMBO J 39, e102729.

Ninomiya K, Hirose T (2020). Short tandem repeat-enriched architectural RNAs in nuclear bodies: functions and associated diseases. Noncoding RNA 6, 6.

Prasanth KV, Prasanth SG, Xuan Z, Hearn S, Freier SM, Bennett CF, Zhang MQ, Spector DL (2005). Regulating gene expression through RNA nuclear retention. Cell 123, 249–263.

Sabari BR, Dall'Agnese A, Boija A, Klein IA, Coffey EL, Shrinivas K, Abraham BJ, Hannett NM, Zamudio AV, Manteiga JC (2018). Coactivator condensation at super-enhancers links phase separation and gene control. Science 361, eaar3958.

Sasaki YT, Ideue T, Sano M, Mituyama T, Hirose T (2009). MENepsilon/beta noncoding RNAs are essential for structural integrity of nuclear paraspeckles. Proc Natl Acad Sci USA 106, 2525–2530.

Satoh D, Hirose T, Harita Y, Daimon C, Harada T, Kurihara H, Yamashita A, Ohno S (2014). aPKCλ maintains the integrity of the glomerular slit diaphragm through trafficking of nephrin to the cell surface. J Biochem 156, 115–128.

Shevtsov SP, Dundr M (2011). Nucleation of nuclear bodies by RNA. Nat Cell Biol 13, 167–173.

Shin Y, Brangwynne CP (2017). Liquid phase condensation in cell physiology and disease. Science 357, eaaf4282.

Staněk D, Fox AH (2017). Nuclear bodies: news insights into structure and function. Curr Opin Cell Biol 46, 94–101.

Sunwoo H, Dinger ME, Wilusz JE, Amaral PP, Mattick JS, Spector DL (2009). MEN epsilon/beta nuclear-retained non-coding RNAs are up-regulated upon muscle differentiation and are essential components of paraspeckles. Genome Res 19, 347–359.

Tafforeau L, Zorbas C, Langhendries JL, Mullineux ST, Stamatopoulou V, Mullier R, Wacheul L, Lafontaine DL (2013). The complexity of human ribosome biogenesis revealed by systematic nucleolar screening of pre-rRNA processing factors. Mol Cell 51, 539–551.

Tohsato Y, Monobe K, Suzuki K, Hayano T, Kawasaki I, Ito M (2012). Comparative proteomic analysis reveals differentially expressed proteins in Caenorhabditis elegans pgl-1 mutants grown at 20°C and 25°C. J Proteomics 75, 4792–4801.

Uversky VN (2017). Intrinsically disordered proteins in overcrowded milieu: membrane-less organelles, phase separation, and intrinsic disorder. Curr Opin Struct Biol 44, 18–30.

Wang M, Herrmann CJ, Simonovic M, Szklarczyk D, Mering CV (2015). Version 4.0 of PaxDb: protein abundance data, integrated across model organisms, tissues, and cell lines. Proteomics 15, 3163–3168.

Yamazaki T, Nakagawa S, Hirose T (2019). Architectural RNAs for membraneless nuclear body formation. Cold Spring Harb Symp Quant Biol 84, 227–237.

Yamazaki T, Souquere S, Chujo T, Kobelke S, Chong YS, Fox AH, Bond CS, Nakagawa S, Pierron G, Hirose T (2018). Functional domains of NEAT1 architectural lncRNA induce paraspeckle assembly through phase separation. Mol Cell 70, 1038–1053.e1037.

Yoshizawa T, Ali R, Jiou J, Fung HYJ, Burke KA, Kim SJ, Lin Y, Peeples WB, Saltzberg D, Soniat M, *et al*. (2018). Nuclear import receptor inhibits phase separation of FUS through binding to multiple sites. Cell 173, 693–705.e622.

Zhao W, Kruse JP, Tang Y, Jung SY, Qin J, Gu W (2008). Negative regulation of the deacetylase SIRT1 by DBC1. Nature 451, 587–590.